Static and dynamic transport of light close to the Anderson localization transition

J. Gómez Rivas, R. Sprik, and A. Lagendijk
Van der Waals-Zeeman Instituut, Universiteit van Amsterdam, 1018 XE Amsterdam, The Netherlands

L. D. Noordam and C. W. Rella*
FOM-Institute for Atomic and Molecular Physics (AMOLF), Kruislaan 407, 1098 SJ Amsterdam, The Netherlands
(Received 16 October 2000; published 29 March 2001)

Anderson localization of light refers to an inhibition of wave transport in scattering media due to the interference of multiple scattered waves. We present wavelength dependent midinfrared optical transport measurements in slabs of randomly packed germanium (Ge) micron-sized particles, using a free electron laser as a tunable source of pulsed radiation. Because of their high refractive index and low absorption, Ge and similar semiconductors are excellent systems to study Anderson localization of light. To characterize the samples fully, we have employed several complementary optical techniques: total diffuse transmission, total diffuse reflection, coherent transmission, and time-resolved speckle interferometry. In this way we obtained the scattering (l_s) and transport (l) mean free paths, the absorption coefficient (α), the diffusion constant (D), and the energy transport velocity (v_e). These measurements have been made as a function of midinfrared wavelength, so that the scattering cross section and absorption coefficients can be varied in the same samples. We found that the Ge samples are close ($kl_s \approx 3$) to the localization transition, but still above it. Our measurements of l_s and l suggest that l is renormalized due to interference at the proximity of the localization transition. We also found that the diffusion constant is significantly reduced in samples thinner than $\approx 7l$.

DOI: 10.1103/PhysRevE.63.046613 PACS number(s): 42.25.Dd, 72.15.Rn, 42.25.Hz

I. INTRODUCTION

Multiple scattering of light in random media of scatterers is a phenomenon encountered daily. Clouds, milk, sand, paper, etc. are examples of media in which multiple scattering of light occurs. In these media the scattering is weak, i.e., $kl_s \gg 1$, where k is the wave vector of the light in the medium, and l_s is the scattering mean free path or the average distance between scattering events. In the case of weak scattering the transport of light may be well described by means of the diffusion approximation [1]. The diffusion approach neglects the interference of light propagating along different paths inside the medium. If the disorder is increased, l_s becomes smaller. For isotropic scatterers, if l_s becomes less than the critical mean free path $l_c \approx 1/k$, the wave cannot perform a complete oscillation in between scattering events. In this regime interference cannot be neglected, and the diffusion description of the propagation of light breaks down. Anderson localization is then established [2]. Localization refers to an inhibition of wave transport in scattering media due to the interference of multiple scattered waves. The transition between the diffusion regime and the localization regime for light is similar to the metal-insulator transition observed at low temperatures in highly doped semiconductors [3]. Anderson localization is essentially a wave phenomenon; therefore, it holds for all kind of waves [4,5], i.e., electrons, electromagnetic waves, and acoustic waves.

To approach the localization transition, i.e., $l_s \approx l_c$ or equivalently $kl_s \approx 1$, also known as the Ioffe-Regel criterion for localization [6], l_s needs to be reduced. The scattering mean free path is inversely proportional to the scattering cross section σ_s of the scatterers. For light, σ_s is maximal when (a) the size of the scatterers is of the order of the wavelength λ; and (b) the refractive index contrast is high, i.e., micron-sized particles of a high refractive index, n, material surrounded by a low refractive index material. The role of absorption in the localization process is still under debate. It is believed that absorption strongly influences the localization of light, and ultimately destroys it [4,7], although in other works [8,9] it is argued that absorption introduces only trivial effects and does not alter the essential behavior of the transport of light. The competition between localization and absorption is very interesting to study. For electronic systems absorption is not present, since the number of electrons is conserved. Difficulties in realizing a medium with the described optical characteristics is the reason why only a few experiments reported localization of classical waves in three-dimensional systems [7,10–12].

Recently, localization of near infrared light was reported in a powder of gallium arsenide (GaAs) particles [10]. Intrinsic GaAs has a high refractive index ($n \approx 3.5$), and very low absorption in the near infrared. Nevertheless, the interpretation of these measurements has been questioned by the possibility of optical absorption introduced during the sample preparation [13]. Enhanced backscattering measurements of visible light on macroporous gallium phospide (GaP) samples [12] showed an effect attributed to the proximity of the localization transition. GaP has $n \approx 3.3$, and it was clearly shown that absorption was absent in this system [12]. We have focused our efforts on germanium (Ge) powder. Germanium is the semiconductor with the highest refractive index in the near and midinfrared ($n \approx 4$), and the absorption

*Present address: Informed Diagnostics, 1050 Duane Avenue, Suite I, Sunnyvale, CA 94086.

of intrinsic Ge is very low in this spectral region [14]. Hence Ge is a good candidate for preparing a material in which infrared light is localized.

In this paper we present wavelength dependent midinfrared (4.5–8 μm) transmission and reflection measurements in randomly close packed micron-sized Ge particles (Ge powder). Tuning λ allows us to vary the scattering cross section (hence l_s), since it depends on the relationship between the particle size and the optical wavelength. To characterize the optical properties of the samples fully, we have performed a complete series of optical transport experiments.

(1) Coherent transmission [15]: by measuring the decay in the intensity of the spatially coherent fraction of the transmitted beam, we obtained a direct measurement of the scattering mean free path l_s. These are, to our knowledge, the first measurements of l_s in a strongly scattering medium.

(2) Total diffuse transmission and reflection [15]: the measurement of the diffusely transmitted and reflected light allows us to obtain two important parameters—the transport mean free path l or the average distance over which the direction of propagation of the light is randomized, and the absorption coefficient α. Close to the Anderson localization transition, l is expected to be renormalized due to interference, becoming smaller than l_s. When $l_s = l_c$, the transport of light is inhibited and $l = 0$.

(3) Time-resolved speckle interferometry: in conjunction with the experiments described above, speckle interferometry provides a means of measuring dynamic transport quantities such as the diffusion constant D and the energy velocity v_e.

This paper is organized as follows. In Sec. II we review the theoretical framework of the propagation of light in the weak scattering limit and at the proximity of the localization transition. The Ge powder sample preparation method is described in Sec. III. In Sec. IV we present the optical measurements. In Sec. V we discuss our results, and we compare them with previous works. The conclusions are summarized in Sec. VI. In the Appendix we discuss the influence of an absorbing substrate on the extrapolation lengths of a random medium of scatterers.

II. THEORY

The transport of light in a random medium of scatterers in the weak scattering limit, $kl_s \gg 1$, is well described by the radiative transfer equation (RTE) [1]. In the RTE, interference of waves propagating along different paths is neglected. Unfortunately, the RTE cannot be solved analytically in most cases. An alternative to the RTE is the diffusion approximation, for which analytical solutions are easily found [1,16]. The validity of the diffusion approximation to describe the propagation of classical waves in multiple scattering media has been experimentally demonstrated for light [17], as well as for sound [18]. The diffusion approximation, besides neglecting interference, considers an almost isotropic distribution of the propagation direction of the light intensities. The energy density inside the sample, ρ, is then given by

$$\frac{\partial \rho}{\partial t} - D_B \frac{\partial^2 \rho}{\partial z^2} = I_0 \delta(z - z_p) - \frac{D_B}{L_a^2}\rho. \tag{1}$$

The diffusion constant is defined as $D_B = v_e l_B/3$, where v_e is the energy transport velocity in the medium [19], and l_B is the Boltzman mean free path or the transport mean path in the absence of interference. The absorption length L_a is the average distance between the beginning and end points of paths of length α^{-1}. The relation between L_a and α is given by $L_a = \sqrt{l_B/3\alpha}$. In Eq. (1), the incoming energy flux at the boundary $z = 0$ is replaced by a source of diffuse radiation of strength, I_0, equal to the incident flux and located at the plane $z = z_p$ [20].

If we consider a medium with lateral dimensions x and y, much larger than its transverse dimension z, the boundary conditions of the diffusion equation are determined considering that the diffuse fluxes going into the sample at $z = 0$ and L are due to a finite reflectivity at the boundaries [21,22],

$$\rho - z_{0_1} \frac{\partial \rho}{\partial z} = 0 \quad \text{at } z = 0, \tag{2}$$

$$\rho + z_{0_2} \frac{\partial \rho}{\partial z} = 0 \quad \text{at } z = L, \tag{3}$$

where $z_{0_{1,2}} = (2l_B/3)(1 + \overline{R_{1,2}})/(1 - \overline{R_{1,2}})$, and $\overline{R_{1,2}}$ are the polarization and angular averaged reflectivities of the boundaries [22]. Index 1 refers to the interface at which the incoming beam is incident ($z = 0$), while index 2 is ascribed to the opposite interface ($z = L$). In the nonabsorbing limit ($L_a \to \infty$), Eqs. (2) and (3) are equivalent to extrapolate ρ to 0 at a distance $z_{0_{1,2}}$ outside the sample surface. Therefore, $z_{0_{1,2}}$ are called the extrapolation lengths. The extrapolation factors $\tau_{0_{1,2}}$ are defined as $\tau_{0_{1,2}} = z_{0_{1,2}}/l_B$.

Due to multiple scattering, which increases the transit time of the light through the sample, a transmitted pulse is broadened. The long time tail of the pulse, obtained by solving Eq. (1) with the boundary conditions (2) and (3), is given by an exponential decay with a characteristic decay time [23]:

$$\frac{1}{\tau} = D_B \left(\frac{\pi^2}{(L + z_{0_1} + z_{0_2})^2} + \frac{1}{L_a^2} \right). \tag{4}$$

From Eq. (4) it is clear that dynamic or time-resolved measurements allow one to obtain the light diffusion constant in a disordered scattering media.

The stationary diffuse transmission and reflection or total transmission, $T_d(z_p)$, and total reflection, $R_d(z_p)$, are given by [24–26]

$$T_d(z_p)=\frac{\sinh(z_p/L_a)+(z_{0_1}/L_a)\cosh(z_p/L_a)}{(1+z_{0_1}z_{0_2}/L_a^2)\sinh(L/L_a)+(1/L_a)(z_{0_1}+z_{0_2})\cosh(L/L_a)}, \tag{5}$$

$$R_d(z_p)=\frac{\sinh((L-z_p)/L_a)+(z_{0_2}/L_a)\cosh((L-z_p)/L_a)}{(1+z_{0_1}z_{0_2}/L_a^2)\sinh(L/L_a)+(1/L_a)(z_{0_1}+z_{0_2})\cosh(L/L_a)}. \tag{6}$$

In Eqs. (5) and (6) the source of diffuse radiation is located at a fixed plane $z=z_p$. However, in a real system the source is extended as it is the scattered light out of the incoming coherent beam. We need to incorporate the spatial extension of the source to analyze the measurements correctly. The intensity of the coherent beam decays exponentially as it penetrates inside the sample with a characteristic length given by l_s. Therefore, the transmission of the coherent beam is given by

$$T_{\mathrm{coh}}=e^{-L/l_s}. \tag{7}$$

If the scattering is anisotropic, one scattering event is not enough to randomize the direction of the propagation of the light; in other words one scattering event does not fully convert the ballistic propagation of the light into diffuse propagation. The number of scattering events required for a full conversion is

$$\frac{l_B}{l_s}=\frac{1}{1-\langle\cos\vartheta\rangle}, \tag{8}$$

where $\langle\cos\vartheta\rangle$ is the average of the cosine of the scattering angle. In Eq. (8) we assume nonabsorbing scatterers. If the scattering is isotropic, $\langle\cos\vartheta\rangle=0$, the direction of propagation of simply scattered light is fully randomized. For systems formed by (nearly) isotropic scatters Eqs. (5) and (6) can be properly weighted with an exponential source distribution:

$$T_d=\int_0^{L/l_B}T_d(z_p)e^{-z_p}dz_p, \tag{9}$$

$$R_d=\int_0^{L/l_B}R_d(z_p)e^{-z_p}dz_p. \tag{10}$$

Equations (9) and (10) represent the diffuse total transmission and reflection of a disordered slab of isotropic scatterers that is illuminated at one side, and they are the basis for the analysis of the total transmission and reflection measurements.

In the limit $l_B\ll L\ll L_a$, T_d scales with the inverse of the sample thickness, L. This is equivalent to the familiar Ohm's law for the conductance in electronic systems. In the limit $l_B\ll L_a\ll L$, T_d decays exponentially with L and with a characteristic length given by L_a [26],

$$T_d=Ae^{-L/L_a}, \tag{11}$$

where

$$A=\frac{2L_a(l_B+z_{0_1})}{L_a^2+(z_{0_1}+z_{0_2})L_a+z_{0_1}z_{0_2}}. \tag{12}$$

As l_s approaches the critical value $l_c\approx 1/k$ at which the Anderson localization transition takes place, the diffusion constant is renormalized by wave interference. According to the scaling theory of localization [27], the renormalization of the diffusion constant may be expressed as a reduction of the transport mean free path, and, for isotropic scatterers, is given by

$$\frac{D}{D_B}=\frac{l}{l_s}=l_s\left(\frac{1}{\xi_0}+\frac{1}{L_a}+\frac{1}{L}\right), \tag{13}$$

where [5]

$$\xi_0=\frac{l_s^2}{l_s-l_c} \tag{14}$$

is the coherence length or the length over which interference is important. On length scales larger than ξ_0 the light resumes its diffusive propagation with a renormalized diffusion constant D and transport mean free path l given by Eq. (13). Therefore, Eqs. (4), (9), and (10) are still valid close to the transition if D_B and l_B are replaced by D and l, respectively. In an infinite and nonabsorbing medium at the transition $\xi_0=\infty$ and $l=0$, which means that the diffusion constant vanishes or that the transport of light is inhibited. In Eq. (13), a finite absorption, given by L_a and sample thickness, L, are included with the same weight as cutoff lengths for ξ_0. This is valid for cube geometry samples. However, most of the experiments in random media of scatterers are done in slab geometry samples or layers of scatterers with x and y dimensions much larger than the thickness. For such samples the contribution of absorption in Eq. (13) is expected to be more important than the finite thickness of the sample, since light paths longer than L_a are removed due to absorption, while paths much longer than L are still possible along the x-y planes. The presence of optical absorption is not by itself a disadvantage. The study of the role that absorption plays in the localization process is very interesting; for instance, an anomalous absorption length close the localization transition has been predicted in weak absorbing media due to the slowing down of the transport of light [4].

III. GE SAMPLES

Germanium is a semiconductor with an energy band gap of 0.62 eV corresponding to $\lambda = 2.0$ μm. The absorption coefficient of intrinsic Ge is very low ($\alpha < 0.1$ cm^{-1}) in the wavelength range 2–15 μm [14]. The lower limit is given by the energy band gap, while the higher limit is due to photon-phonon absorption bands. The refractive index of Ge in this range is very high and nearly constant ($n \approx 4$) [14].

Our starting material for the Ge powder slabs was high purity (99.9999%) Ge (Aldrich 26323-0). We ground 2 g of Ge with a mortar until all pieces were smaller than 1 mm. To reduce the particles size further, we milled them in a planetary micromill using zirconia (ZrO_2) beaker and balls. After milling at low speed during 4 min, 5 ml of spectroscopy grade methanol was added, and the particles in suspension were milled for another minute. We added 25 ml of methanol, and we let the largest particles sediment over 150 s. Only the particles that did not sediment were used in the experiments. A few drops of the suspension were put on calcium fluoride (CaF_2) disk shaped substrates with a diameter of 12.7 mm and 1 mm thick, and we let evaporate the methanol. The resulting samples were firm, and starchy slabs of randomly close-packed Ge particles in an air matrix—in other words, slabs of Ge powder.

The thickness L of the Ge slabs was measured by making scratches at the edges of the samples. With a calibrated microscope with 1-μm-resolution, we focused on the surface of the sample and on the CaF_2 substrate. The thickness is given by the difference between the focus points. In our samples L ranges from 7.4 to 73.2 μm.

To measure the size of the Ge particles, and to check if the samples were homogeneous, we performed scanning electron microscopy. Figure 1(a) is a side view of a Ge sample, along one of the scratches made to measure the sample thickness. In Fig. 2 we schematically represent a sample, the dotted arrow showing the direction of observation of Fig. 1(a). The sample is formed by a top layer of small particles and a bulk of much larger Ge particles. For comparison, in Figs. 1(b) and 1(c) we show photographs of sample upper and lower surfaces, respectively. Energy dispersion x-ray spectroscopy (EDX) measurements on the samples top layer showed that it is mainly formed of Ge, together with a small amount of impurities introduced during the milling. From electron microscope images of several samples we have estimated the thickness of the top layer, d, to be 5 ± 1 μm, and to be constant for all the samples. We also checked that the size of the Ge particles in the sample bulk is the same at different depths, and that the size of the particles is the same in all the samples.

Defining the particle radius as half the maximum distance between parallel tangents to the particle surface [28], we have measured the radius of many particles of the top layer and the sample bulk. In Fig. 3 we plot a histogram of the radius of the particles of the top layer (solid bars) and of the sample bulk (dashed bars). By fitting the histograms with log-normal distribution functions (dotted and solid lines in Fig. 3), the average particle radius in the top layer is found to be 0.19 ± 0.13 μm, and that in the sample bulk to be 0.98 ± 0.68 μm.

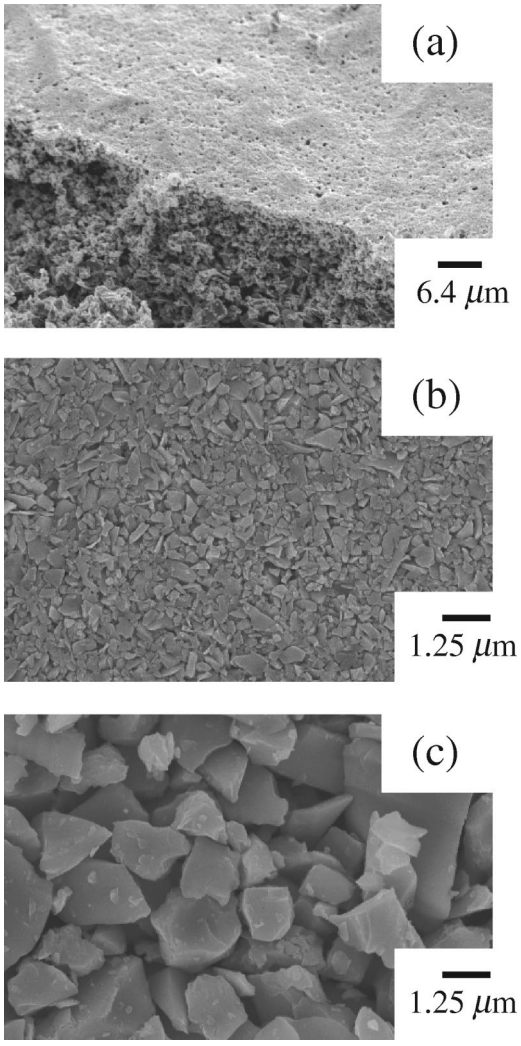

FIG. 1. Scanning electron microscope photographs of the Ge powder samples. (a) Shows a side view of a sample. The direction of observation is marked in Fig. 2 with a dotted arrow. (b) Is the upper surface of the sample, while (c) shows the lower surface. Note that the magnifications in (b) and (c) are the same.

Due to the small size of the particles of the top layer and to its thickness, the scattering in this layer is negligible [29]. Therefore, we may describe the samples as a homogeneous top layer of thickness $d = 5$ μm in which only absorption takes place, and a bulk of Ge particles with a thickness given by $L - d$ where scattering and absorption occur. The absorption in the top layer is characterized by the absorption coefficient α_{TL}. Due to the irregular shape of the Ge particles, their size, and their random orientation, we may consider the scattering in the sample bulk to be nearly isotropic, $l_B \approx l_s$. The absorption coefficient in the bulk is given by α.

IV. MEASUREMENTS

A midinfrared free electron laser (FEL) (FELIX, Rijnhuizen, The Netherlands), was used as tunable source of intense

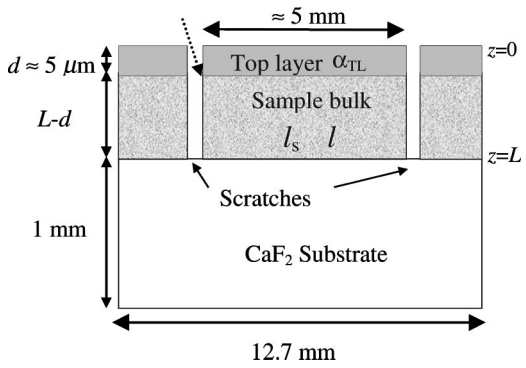

FIG. 2. Schematic representation of a Ge powder sample. The thin top layer is formed by small Ge particles and impurities introduced during the sample preparation. We neglect the scattering in the top layer, which is then characterized only by the absorption coefficient α_{TL}. The sample bulk, formed by larger Ge particles, is characterized by the scattering mean free path l_s, the transport mean free path l, and the absorption coefficient α. The dotted arrow shows the direction of observation in Fig. 1(a). Also, the scratches made on the sample to measure its thickness are represented.

infrared radiation. The full capabilities of this FEL are described elsewhere [30]. The FEL is continuously tunable over a wavelength range of 4.5–200 μm, and generates an intense train of picosecond pulses (micropulses) of ≈ 1-μJ energy each, and a fractional spectral bandwidth of about 1%. Each train of micropulses (called macropulse) contains about 100 micropulses, with an interpulse spacing of 40 ns. In general, the signal from 25 macropulses is averaged at each measurement.

A. Coherent transmission

We first describe the transmission measurements of the coherent beam. The output of the FEL was sent through a beamsplitter, and the reflected beam was directed to a broadband pyroelectric detector. The signal from this detector was used as power reference. A 0.1-cm-diameter iris was placed just before the sample to insure that the FEL beam illuminated only the most homogeneous portion of the sample. At a distance of 120 cm from the sample, and in the direction of the incoming FEL beam, an iris of 0.7-cm-diameter was placed. After the iris a BaF_2 lens focused the transmitted FEL beam onto a sensitive liquid nitrogen cooled mercury cadmium telluride (MCT) detector. The long distance between the sample and the detector insured that the detected diffuse light, transmitted through the sample, was negligible. We measured the transmission of the coherent beam at four wavelengths, $\lambda = 5$, 6.5, 6.9, and 8 μm.

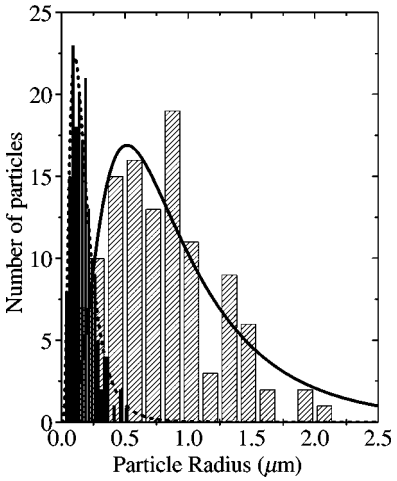

FIG. 3. Histograms of the particle radius in the Ge powder samples. The solid bars correspond to particles of the top layer of the samples. The dashed bars are the histogram of the bulk Ge particles. The dotted and solid lines are fits of the histograms to log-normal distribution functions, from which we obtain the average particle radius.

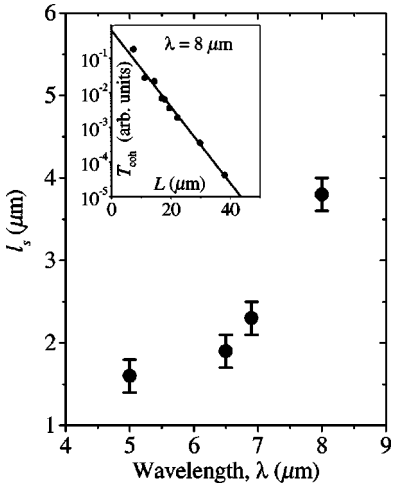

FIG. 4. Scattering mean free path l_s in Ge powder samples as a function of the wavelength, λ. Inset: measurements of the transmission of the coherent beam ($\lambda = 8$ μm) as a function of the sample thickness, L. The line is an exponential fit to the measurements from which we obtain the scattering mean free path ℓ_s. At this particular λ, $\ell_s = 3.8 \pm 0.2$ μm.

In the inset of Fig. 4 we plot the transmission measurements of the coherent beam as a function of the sample thickness at $\lambda = 8$ μm. Clearly the transmission decreases exponentially with the sample thickness. The characteristic length of this decay is l_s. Figure 4 shows l_s as a function of λ. The nearly constant value of l_s at 5, 6.5, and 6.9 μm may be understood in terms of the high polydispersity in the size of the Ge particles. The effect of the polydispersity in the scattering properties of the medium was discussed in Ref. [26]. Only at $\lambda = 8$ μm is l_s significantly larger. It is expected that as λ increases, l_s becomes larger due to the reduction of σ_s. In the limit of λ much larger than the size of the scatterers (Rayleigh limit), $\sigma_s \propto 1/\lambda^4$. In Fig. 5 we plot the localization parameter kl_s as a function of λ. The wave number k is given by $(2\pi/\lambda)n_e$, where n_e is the effective refractive index of the sample bulk. A good estimate of n_e is given by the Maxwell-Garnet effective refractive index [31]. Taking a Ge volume fraction of 40% [10,26], we find $n_e \approx 1.6$ in the measured λ range. As can be seen in Fig. 5, the Ge powder samples are very close to the localization transition (kl_s close to 1), where localization effects, like the

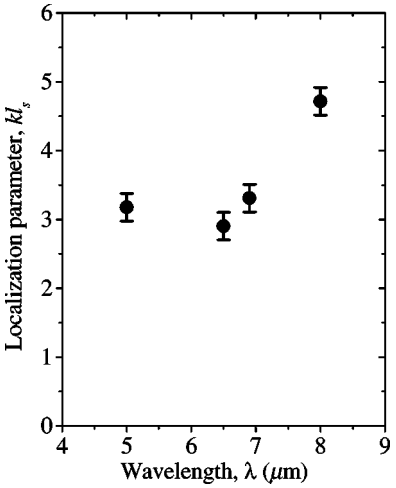

FIG. 5. Localization parameter kl_s in Ge powder samples as a function of the wavelength λ.

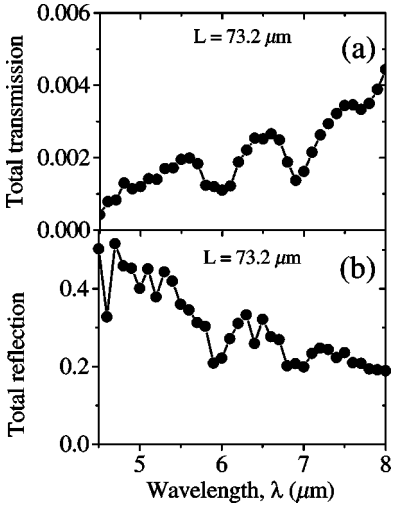

FIG. 6. Normalized total transmission (a) and reflection (b) spectra of a Ge powder sample of thickness 73.2 μm.

renormalization of the transport mean free path, are expected to occur.

B. Diffuse total transmission and reflection

To obtain the transport mean free path l, we measured the total transmission and the total reflection. The total transmission was measured as follows. The output of the FEL was brought to a weak focus of about 0.1 cm at the sample by using two BaF_2 lenses. The sample was mounted at the input of a diffuse gold (infragold) coated integrating sphere (IS) of 10-cm-diameter (Labsphere IS040IG). The IS collects the light transmitted in all directions, allowing us to measure the total transmission. At the output of the IS was a MCT detector. A power reference was simultaneously measured in the same way as described for the coherent beam measurements. The total transmission measurements were normalized by the transmission spectrum of a clean CaF_2 substrate. For the total reflection measurements the FEL beam was sent into the IS through a small input port of 0.3-cm-diameter. The sample was at the opposite side of the IS. Therefore, only the reflected light by the sample was collected by the IS. The reference for the reflection measurements was a thick infragold sample with a diffuse reflection $\approx 96\%$ in the λ range $2-20$ μm. For the total transmission and reflection measurements we made spectral scans in the range $4.5-8$ μm, with steps of 0.1 μm. The lower limit is set by the tunning range of the FEL, while the higher limit is due to CaF_2 absorption.

Figures 6(a) and 6(b) display the normalized total transmission and reflection spectra of the $L=73.2$ μm sample, respectively. At all wavelengths the transmission is very small, but there are some distinct spectral features. The spectra show two distinct narrow absorption bands at 6.0 and 6.9 μm. These two absorption bands are due to vibrational modes of hydrocarbon impurities introduced during the sample preparation. Exploiting the pulsed characteristics of the FEL, we have confirmed stronger absorption at these bands by means of photoacoustic spectroscopy measurements [32].

In the following we show how we deduce l from the total transmission and reflection measurements. In Fig. 7 we plot typical total transmission (a) and total reflection (b) measurements as a function of the sample thickness, L. The measurements of Fig. 7 correspond to $\lambda=8$ μm. To obtain the transport mean free path, we need first to know the extrapolation factors τ_{0_1} and τ_{0_2}. Given the effective refractive index of the Ge powder, $n_e \approx 1.6$, and the refractive index of CaF_2, τ_{0_2} is calculated. Considering the multiple reflections at the CaF_2-air interface [33], we find $\tau_{0_2} \approx 2.7$. To obtain τ_{0_1}, we fit the total transmission measurements of the thickest samples to

$$T = A e^{-\alpha_{\mathrm{TL}} d} e^{-(L-d)/L_a}. \tag{15}$$

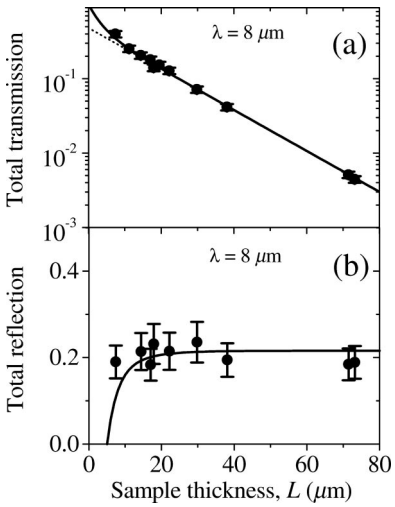

FIG. 7. Total transmission (a) and reflection (b) measurements in Ge powder samples at $\lambda=8$ μm as a function of the sample thickness L. The solid line in (a) is a fit using the diffusion theory. The dotted line (hidden by the solid line except at small L) is an exponential fit to the total transmission of the thickest samples. In (b) the solid line represents a fit of the total reflection measurements using the diffusion theory.

This equation is equivalent to Eq. (11), with the source attenuated by the factor $e^{-\alpha_{\mathrm{TL}}d}$. This attenuation is due to absorption in the sample top layer. For isotropic scatterers, one finds, using Eqs. (11), (12) and (15), that

$$\tau_{0_1}=\frac{-2L_a l_s+A' L_a(L_a+\tau_{0_2} l_s)e^{\alpha_{\mathrm{TL}}d}}{2L_a l_s-A' l_s(L_a+\tau_{0_2} l_s)e^{\alpha_{\mathrm{TL}}d}}, \tag{16}$$

where A' is given by Eq. (15) at $L=d$. The dotted line in Fig. 7(a) represents a fit of Eq. (15) to the $\lambda=8$ μm measurements. From the fit we obtain $A'=0.35\pm0.05$ and $L_a=15.5\pm0.5$ μm. To obtain τ_{0_1} from Eq. (16), we need to know α_{TL}. The total reflection measurements are more sensitive to the absorption in the top layer because the reflected light crosses this layer twice. Therefore, the low reflection exhibited by our samples (only 20% at $\lambda=8$ μm) is mainly due to strong absorption in the top layer. To estimate the absorption coefficient in the top layer, α_{TL}, we fit the total reflection measurements with

$$R=e^{-\alpha_{\mathrm{TL}}d}R_d\int_0^1 e^{-\alpha_{\mathrm{TL}}d/\mu}P(\mu)d\mu, \tag{17}$$

where $\mu=\cos\theta$, and θ is the angle with respect to sample surface normal at which the diffuse reflected light exits the sample bulk. The diffuse reflected light is angular distributed according to $P(\mu)\propto\mu[\frac{2}{3}+\mu/(1+\mu)]$ [34], where we assume that the bulk of the sample and the top layer have the same index of refraction; this is justified, since we know from the EDX measurements that the top layer is mainly formed of Ge, and from the scanning electron microscope photographs that the packing of the particles is similar in both regions. The factor $e^{-\alpha_{\mathrm{TL}}d}$ in Eq. (17) represents an attenuation of the coherent beam due to absorption in the sample top layer, R_d is the diffuse reflection of the sample bulk, and the integral represents the attenuation of the diffuse reflected light due to absorption in the top layer. In Eq. (17) we have considered isotropic scatters, $l_B=l_s$, and have neglected reflections at the sample top layer-air interface. By neglecting these reflections we obtain a higher value of α_{TL} from the fit than the real one. We have determined the overestimation of α_{TL} to be $\approx15\%$. Nevertheless, this overestimation of α_{TL} is irrelevant for the value of the transport mean free path that we will obtain from the fit to the total transmission. The fit of Eq. (17) to the reflection measurements at $\lambda=8$ μm is shown as a solid line in Fig. 7(b). From this fit we obtain $\alpha_{\mathrm{TL}}=0.091\pm0.008$ $\mu\mathrm{m}^{-1}$. To obtain α_{TL} at wavelengths other than $\lambda=5$, 6.5, 6.9, and 8 μm, where we have directly measured l_s, we linearly interpolate the values l_s at intermediate λ. The circles in Fig. 8 represent α_{TL} as a function of λ. In Fig. 9 we plot the wavelength dependence of τ_{0_1}, as obtained from Eq. (16). The lower value of τ_{0_1} at the absorption bands (6.0 and 7.0 μm) should not be attributed to a decrease of the boundary reflectivity, but to an increase of the absorption at the samples top layer (see the Appendix). With the values of τ_{0_1},

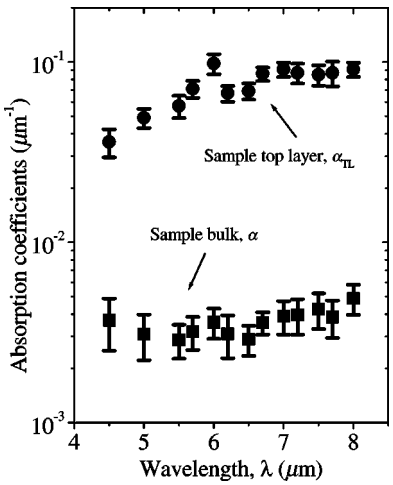

FIG. 8. Circles: absorption coefficient in the Ge powder samples top layer, α_{TL}, as a function of the wavelength λ. Squares: absorption coefficient in the bulk of the samples, α.

τ_{0_2}, α_{TL}, and L_a we can obtain the transport mean free path from the total transmission measurements using the equation

$$T=e^{-\alpha_{\mathrm{TL}}d}(T_d+e^{-(L-d)/l_s}). \tag{18}$$

The solid line in Fig. 7(a) is a fit of the total transmission measurements using Eq. (18). The first term inside the brackets of Eq. (18) is the diffuse total transmission, while the second term is the transmission of the coherent beam. The factor $e^{-\alpha_{\mathrm{TL}}d}$ represents the attenuation of the incoming beam due to absorption in the top layer. The transmission of the coherent beam rapidly decreases with L, being insignificant for thick samples. At $\lambda=8$ μm, with $d=5$ μm, $\tau_{0_1}=1.6$, $\tau_{0_2}=2.7$, $\alpha_{\mathrm{TL}}=0.091\pm0.008$ $\mu\mathrm{m}^{-1}$, and $L_a=15.5\pm1$ μm, we find from the fit $l=3.5\pm0.5$ μm (Table I). At this λ the incident beam is attenuated by more than 30% due to absorption in the top layer. The wavelength dependence of l is plotted in Fig. 10. Consistently with the measurements of l_s, l increases at higher λ due to the reduction of σ_s. The

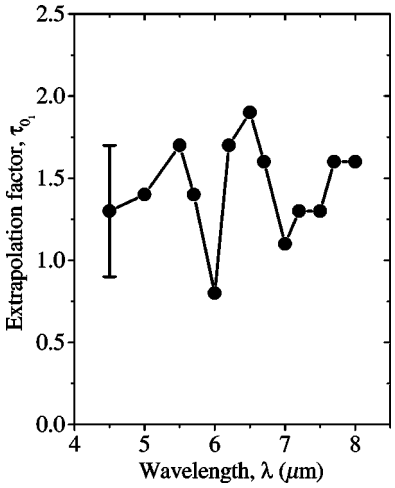

FIG. 9. Extrapolation factor τ_{0_1} of the Ge powder samples as a function of the wavelength λ.

TABLE I. Scattering properties in Ge powder samples at $\lambda = 8\ \mu$m. Scattering mean free path (l_s), localization parameter (kl_s), transport mean free path (l), absorption coefficient in the sample bulk (α), absorption coefficient in the sample top layer (α_{TL}), diffusion constant (D), and energy transport velocity (v_e).

λ (μm)	l_s (μm)	kl_s	l (μm)	α ($10^{-3}\mu m^{-1}$)	α_{TL} ($10^{-2}\mu m^{-1}$)	D (m^2/s)	v_e (10^7 m/s)
8	3.8 ± 0.2	4.7 ± 0.2	3.5 ± 0.5	4.9 ± 0.9	9.1 ± 0.8	$\simeq 26$	$\simeq 5.5$

squares in Fig. 8 are the absorption coefficient, $\alpha = l/(3L_a^2)$, in the bulk of the sample. We see that, although $\alpha^{-1} \gg l$, significant absorption has been introduced in the sample bulk during the sample preparation. Most likely we have created surface defects in the Ge particles and introduced impurities during the milling, giving rise to an increase of the absorption. The absorption is stronger in the top layer where the size of the particles is smaller, and where we have measured by EDX the presence of impurities from the mill.

C. Time-resolved speckle interferometry

From the optical experiments described above, we have obtained high quality measurements of the absorption coefficient and the transport and scattering mean free paths in the bulk material, as well as the absorption in the top layer of fine particles. Unfortunately, as these are static measurements, it is not possible to extract from them dynamical transport quantities such as the diffusion constant D and the energy transport velocity v_e. To study these dynamical properties, we have employed time-resolved speckle interferometry, a technique which takes advantage of the picosecond pulse structure of the FEL, to map out the envelope of the diffusely transmitted pulse interferometrically. Upon entering the scattering medium, the incoming optical pulse will undergo a temporal delay and broadening due to multiple scattering events, which increase the light transit time in the samples. A schematic of the experimental apparatus used to perform this experiments is shown in Fig. 11. The sample was mounted in one of the arms of a Mach-Zender interferometer. The majority of the infrared power was focused weakly to a 1-mm spot at the sample. A small cone of the diffuse transmission far in angle ($\approx 20°$) from the coherently transmitted beam propagated about 1 m, and then was collected by a 10-mm-focal length lens onto a MCT detector. A variable iris was placed before this lens such that the detector collected light from only a single speckle spot. A 10% reflecting beamsplitter, located before the sample, created the copy of the input optical pulse that was sent along the other arm of the interferometer. This reference pulse was directed down a variable optical delay line before it was combined colinearly, on a second beamsplitter just before the iris, with the diffusely transmitted pulse. As the optical delay was scanned, the detector recorded the interferogram between the scattered pulse and the reference pulse. As in the other measurements, a reference detector was used to normalize laser fluctuations. An added complication was atmospheric absorption, which causes temporal pulse breakup due to the relatively narrow absorption lines. For this reason, time-resolved measurements were made at just two wavelengths, 4.5 and 8 μm, where atmospheric absorption is marginal.

In the inset to Fig. 12, we display a small portion of a typical interferogram, taken at $\lambda = 4.5\ \mu$m on a 17-μm-thick sample. The oscillations at the optical frequency are clearly visible. In the analysis of these data we take advantage of the fact that oscillations in the interferogram have a well-defined carrier frequency. The data are analyzed further by taking the power spectrum of a narrow

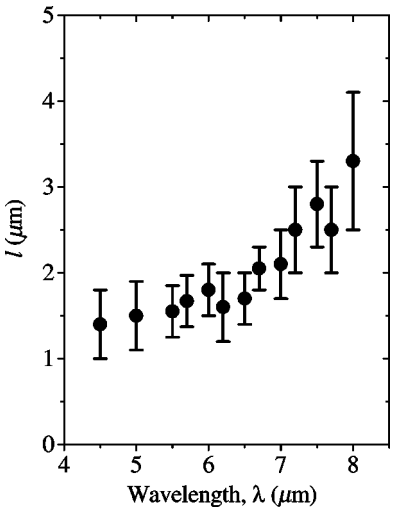

FIG. 10. Transport mean free path l in the bulk of Ge powder samples as a function of the wavelength λ.

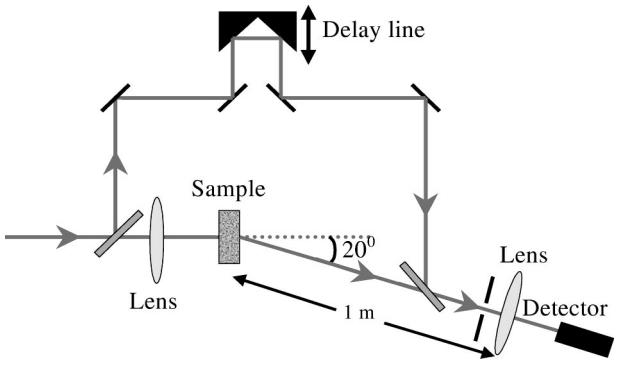

FIG. 11. Schematic representation of the setup used for the time-resolved speckle interferometry measurements. The FEL light was sent into a Mach-Zender interferometer with the sample in one of its arms. The undistorted or reference pulse traveled along the other arm, in which a delay line allowed a change of the optical path length. Both pulses were recombined at the exit of the interferometer. To avoid detecting the coherently transmitted beam, the detector was placed at an angle of 20° with respect to the incident beam direction.

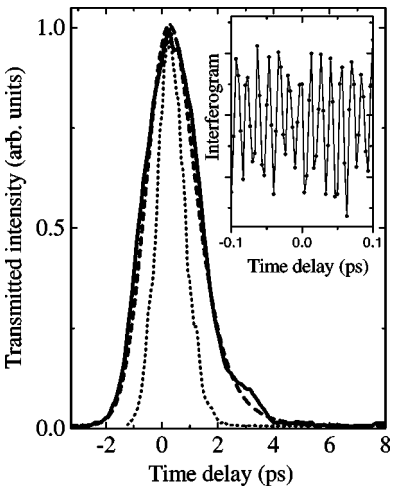

FIG. 12. Transmitted intensity through a Ge powder sample of thickness $L=17$ μm at $\lambda=4.5$ μm (solid line) as a function of the time delay introduced by the delay line of the Mach-Zender interferometer. The dashed line is a fit using classical diffusion theory, convoluted with a Gaussian function, which takes into account the instrument response. The dotted line is the incident pulse shape. The maxima of both pulses have been normalized to the same time delay. The inset is a portion of the interferogram from which the transmitted intensity is reconstructed.

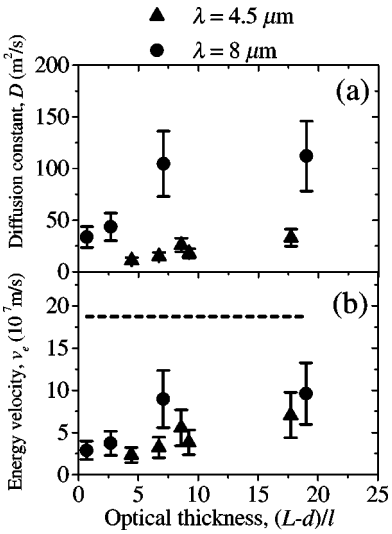

FIG. 13. (a) Diffusion constant D of light at $\lambda=4.5$ μm (triangles) and $\lambda=8$ μm (circles) in Ge powder samples as a function of the sample optical thickness. (b) Energy transport velocity in the same samples and at the same wavelengths. The straight dashed line it the phase velocity in an homogeneous medium with a refractive index equal to the effective refractive index of the Ge powder samples.

(200 fs) time slice of the interferogram, and integrating this spectrum in a narrow (5%) window in the vicinity of the carrier frequency. Due to the coherent nature of the incoming light, the resulting interferogram of a given speckle will have large amplitude and phase fluctuations as functions of the optical delay. It is therefore necessary to average over several speckles for each sample thickness and at each wavelength. This process smooths out the phase and amplitude fluctuations caused by the interference of different paths, leaving only the overall intensity envelope of the diffusely transmitted beam. The result of this averaging process is shown by the solid line in Fig. 12. As expected, the data exhibit a smooth rise time governed primarily by the incident optical pulse length, and a slower decay time due to multiple scattering. The narrower feature (dotted line) is the incoming pulse shape, which was measured using the same setup except with the sample replaced by a thin piece of weakly scattering paper. Note that this pulse is substantially shorter in duration (about 33%) than the transmitted pulse, with a much sharper decay time. The maxima of the transmitted pulses in Fig. 12 have been normalized to the same time delay. Small setup realignments between different samples, necessary to increase the signal-to-noise ratio of the interferogram, made it impossible to extract useful information from pulse delay time. However, the diffusion constant may be obtained from the pulse broadening.

According to diffusion theory [Eq. (4)], The long-time tail of the pulse can be modeled by an exponential decay. Therefore, we fit the time-resolved data with an exponential decay convoluted with a Gaussian function which takes into account the instrument response (the dashed line in Fig. 12). The Gaussian width depends on the incoming pulse duration. The characteristic decay time constant is given by

$$\frac{1}{\tau}=D\left(\frac{\pi^2}{(L-d+z_{0_1}+z_{0_2})^2}+\frac{1}{L_a^2}\right). \tag{19}$$

This expression may be used to obtain the diffusion constant D, using the values of L_a and z_{0_1} obtained from the static measurements described above. The extrapolation length z_{0_2} is equal to $1.1l$, corresponding to the interface sample-CaF_2 substrate. For the time-resolved measurements the reflected light at the CaF_2-air interface does not need to be considered, since this reflected light is detected at later times. Due to the narrow spectral width of the pulse, dispersion in the sample top layer may be neglected. In Fig. 13(a) we plot D as a function of sample optical thickness, $(L-d)/l$, at 4.5 μm (triangles) and 8 μm (circles). For samples thinner than $\approx 7l$, the diffusion constant is significantly reduced. We discuss the optical thickness dependence of D in Sec. V. As expected, the diffusion constant is smaller at shorter λ, where the scattering is stronger.

Using the expression $D=v_e l/3$ and the values obtained for l from the total transmission and reflection analysis, the energy transport velocity v_e is acquired. It is well known that the energy velocity (the rate at which the energy is transported) may be significantly slower than the phase and group velocities due to scattering resonances [19]. The derived values of the energy velocity are plotted in Fig. 13(b), along with the expected phase velocity from our estimate of the index of refraction (dashed line). The large difference between the energy and phase velocities is clear in Fig. 13(b) (more than a factor 2 and 3 at $\lambda=8$ and 4.5 μm, respectively, for samples thicker than $7l$). The scattering properties of the Ge samples at $\lambda=8$ μm obtained from the static and dynamic measurements are summarized in Table I.

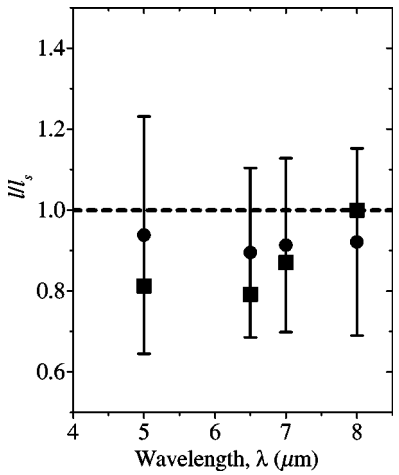

FIG. 14. Circles: transport mean free path l of light of wavelength λ in the Ge powder samples, divided by the scattering mean free path l_s. Squares: expected renormalization of l due to interference assuming that the localization transition is at $l_s=\lambda/2\pi n_e$ and $n_e=1.6$.

V. DISCUSSION

In Fig. 14 we display as circles the ratio of the transport and scattering mean free paths obtained from the static measurements. The values of l/l_s are smaller than 1, which can be only understood by considering the renormalization of l due to the proximity of the localization transition. For comparison, in Fig. 14 we also plot (squares) the expected renormalization of l according to scaling theory [Eq. (13)], assuming $l_c=2\pi n_e/\lambda$ and $n_e=1.6$, and considering only the absorption as a cutoff of the coherent length ξ_0. However, the large error in the determination of l, related to the complicated structure of the samples and to the estimation of the extrapolation factor τ_{0_1}, makes it impossible to prove localization effects unambiguously. In our analysis to find τ_{0_1}, we fix l to l_s in Eqs. (16) and (17), obviating any localization effect.

In Ref. [26] the energy density coherent potential approximation [35] was used to calculate the scattering properties of an infinite system of polydisperse silicon spheres. As a result of the polydispersity, the resonances in l_s in the monodisperse system were smoothed out, and l_s became, in general, larger in the polydisperse medium. Therefore, to further approach the localization transition in Ge samples, it is necessary to reduce the polydispersity.

A great improvement in the reduction of absorption may be achieved by annealing the Ge particles after the milling. To eliminate the hydrocarbon absorption bands at 6 and 6.9 μm, we propose the substitution of methanol as solvent by carbon tetrachloride (CCl_4) or carbon disulfide (CS_2).

Although the determination of l in the Ge samples from the total transmission and reflection measurements is very involved due to the top layer, we have unambiguously determined l_s from the decay in intensity of the coherent beam. These last measurements are unaffected by the reflectivity at the boundaries, and therefore they are independent of τ_{0_1} and τ_{0_2}. We find values of kl_s close to the localization transition but still above it. This is a striking result since in Ref. [10] strong localization ($kl_s<1$) of near infrared light was reported in nonabsorbing GaAs powder. The refractive index of GaAs ($n\approx3.5$) is lower than the one of Ge, and the polydispersity in the samples of Ref. [10] is comparable to the polydispersity in the Ge samples. Also, the size of the particles relative to the measured λ is comparable in both works. In Ref. [26] near infrared total transmission through Si ($n\approx3.5$) powder was measured. These measurements were fully described by using the diffusion approximation. In that work it was argued that a difference in the connectivity between the Si and GaAs particles (due to the different shape of the particles) could be the reason why localization was absent in the Si samples. However, the shapes of the Ge and GaAs particles are similar and, therefore, we also expect a similar connectivity between the particles in both samples. At this moment it is not clear why localization is apparent in GaAs powder but absent in similar samples of Ge powder. More experimental and theoretical work must be done in the GaAs samples to confirm the results of Ref. [10]. A feasible experiment, as clearly shown in Ref. [36], consists of filling the air voids in the GaAs samples with a nonabsorbing liquid and measuring the total transmission. The reduction of the refractive index contrast should be enough to prevent localization, and the total transmission should obey the diffusion approximation with an absorption length larger than the samples thickness. This could confirm that the deviation in the measurements of Ref. [10] from diffusion theory are due to localization.

In Fig. 13(a), where the diffusion constant obtained from the dynamic measurements is plotted versus the sample thickness, we see that D is significantly reduced in samples thinner than $\approx 7l$. Similar optical experiments carried out in TiO_2 powder [37] showed the same thickness dependence of D. Acoustic frequency correlation measurements in samples of glass beads immersed in water [38] are also consistent with a reduced D in thin samples. It is important to note that the values of D given in Fig. 13(a) are obtained from the long time tail of the transmitted pulse, where the diffusion equation is expected to hold even for thin samples. A possible explanation for the nonconstant value of D is given in Ref. [38]. The long time tail intensity in the thin samples is due to light that has mainly traveled along the x-y plane. The reduced dimensionality likely makes interference important, which is not taken into account by the diffusion equation. Therefore, the diffusion approach underestimates D in thin samples.

VI. CONCLUSIONS

We have studied the wavelength dependence of the scattering properties of randomly close-packed micron-sized germanium particles, i.e., Ge powder. By measuring in the mid-infrared the decay in intensity of a free electron laser beam as it crossed the samples, we obtain the scattering mean free path l_s. Our samples are close to the localization transition but still above it. This is an unexpected result, since Anderson localization of light was reported [10] in similar samples of lower refractive index material, GaAs. We have also mea-

sured the total transmission and reflection of the Ge powder samples obtaining the transport mean free path, l, and the optical absorption in the samples. During the sample preparation we introduce significant absorption. Our measurements suggest a renormalization of l due to the proximity to the localization transition. However, the large error in the determination of l, related to the complicated structure of the samples, makes it impossible to exclude localization effects in the Ge samples unambiguously. To approach the localization transition it is necessary to reduce the high polydispersity in the Ge particle size. We have also performed time-resolved speckle interferometry, obtaining the light diffusion constant D and the energy transport velocity v_e for different sample thicknesses. It is found that D is significantly reduced in samples thinner than $\approx 7l$, confirming previous experimental works [37,38].

ACKNOWLEDGMENTS

We gratefully acknowledge the skillful assistance by the FELIX staff, in particular A.F.G. van der Meer. We are also grateful to R.L.W. Popma for the EDX measurements, W. Takkenberg for the SEM photographs, and R.M.A. Heeren and M. Geldof for FTIR reflection measurements. J.G.R. acknowledges financial support from the European Union through the TMR program. This work was part of the research program of the Stichting voor Fundamenteel Onderzoek der Materie (Foundation for Fundamental Research on Matter) and the Stichting Technische Wetenschappen (Technology Foundation), and was made possible by financial support from the Nederlandse Organisatie voor Wetenschappelijk Onderzoek (Netherlands Organization for the Advancement of Research).

APPENDIX: EXTRAPOLATION LENGTH WITH AN ABSORBING SUBSTRATE

The calculation of the reflectance for a double interface or a substrate was done in Ref. [33]. Here we generalize this calculation for the case of absorbing substrates. The top layer of our samples may be considered as a thin absorbing substrate. With the values of the reflectance the extrapolation factors may be calculated. We assume a weakly or nonabsorbing multiple scattering sample that is on an absorbing substrate of thickness h. The effective refractive index of the medium is given by n_e, while the substrate has a complex refractive index $n_s^c = n_s + i\kappa_s$. If $\kappa_s \ll n_s$ the absorption coefficient of the substrate is given by $\alpha_s = 2\pi\kappa_s/\lambda$. The transmitted fraction $T_{ab}(\theta_1)$ of the diffuse light incident at the interface sample-substrate at angle θ_1 (see the inset of Fig. 15) is refracted according to Snell's law, and undergoes a ballistic propagation along the substrate at an angle θ_2. The intensity of the transmitted fraction in attenuated by the factor $e^{-\alpha_s h/\cos\theta_2}$, due to absorption in the substrate. The light reaching the substrate-air interface may be reflected with a probability given by the Fresnel reflection coefficient $R_{bc}(\theta_2)$. The reflected fraction reaches the interface substrate sample, after being attenuated, where it may be reflected, etc. Considering these multiple reflections at both interfaces, the reflection coefficient of the substrate is given by

$$R(\theta) = R_{ab}(\theta_1) + \frac{T_{ab}(\theta_1)R_{bc}(\theta_2)R_{ba}(\theta_2)e^{-2\alpha_s h/\cos\theta_2}}{1 - R_{ba}(\theta_2)R_{bc}(\theta_2)e^{-2\alpha_s h/\cos\theta_2}}. \tag{A1}$$

In Eq. (A1) the indexes a, b, and c stand for media a, (sample), b (substrate), and c (outside medium), as illustrated in the inset of Fig. 15, and, for instance, R_{ab} is the Fresnel reflection coefficient of the interface between media a and b. With the reflection coefficient, given by Eq. (A1), the extrapolation factor τ_0 can be calculated following the procedure described in Ref. [22].

In Fig. 15 we plot the extrapolation factor as function of $(h\alpha_s)^{-1}$ calculated with $n_e = n_s = 1.6$ and, for simplicity, with the Fresnel reflection coefficients calculated for dielectric media. As the absorption in the substrate becomes stronger, τ_0 becomes smaller. The reason for the decrease of τ_0 is the lower light intensity that reaches the substrate-air interface due to absorption in the substrate.

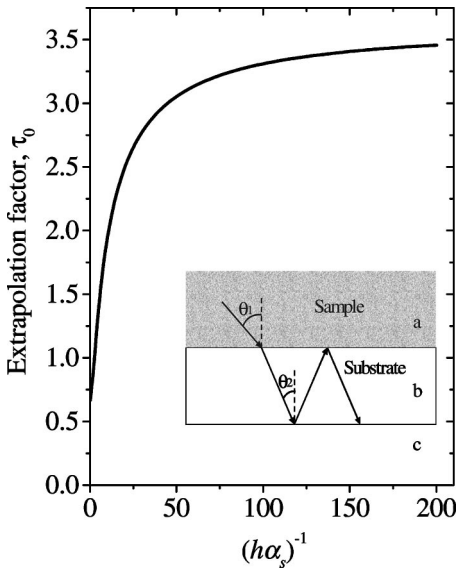

FIG. 15. Extrapolation factor τ_0 of a double interface or substrate, as a function of $(h\alpha_s)^{-1}$, where h is the thickness of the substrate and α_s its absorption coefficient. Inset: the light exiting the sample (medium a) with an angle θ_1 is refracted according to Snell's law. It propagates through the substrate (medium b), being attenuated due to absorption. At the interface between media b and c the light may be reflected with a probability giving by the Fresnel reflection coefficient. The total reflectivity of the substrate is given by the multiple reflections at both interfaces.

[1] A. Ishimaru, *Wave Propagation and Scattering in Random Media* (Academic Press, New York, 1995).
[2] P. W. Anderson, Phys. Rev. **109**, 1492 (1958).
[3] B. Kramer and A. Mackinnon, Rep. Prog. Phys. **56**, 1469 (1993).
[4] S. John, Phys. Rev. Lett. **53**, 2169 (1984).
[5] P. W. Anderson, Philos. Mag. B **52**, 505 (1985).
[6] A. F. Ioffe and A. R. Regel, Prog. Semicond. **4**, 237 (1960).
[7] N. Garcia and A. Z. Genack, Phys. Rev. Lett. **66**, 1850 (1991).
[8] R. L. Weaver, Phys. Rev. B **47**, 1077 (1993).
[9] M. Yosefin, Europhys. Lett. **25**, 675 (1994).
[10] D. S. Wiersma, P. Bartolini, A. Lagendijk, and R. Righini, Nature (London) **390**, 671 (1997).
[11] Z. Q. Zhang, C. C. Wong, K. K. Fung, Y. L. Ho, W. L. Chan, S. C. Kan, T. L. Chan, and N. Cheung, Phys. Rev. Lett. **81**, 5540 (1998).
[12] F. J. P. Schuurmans, M. Megens, D. Vanmaekelbergh, and A. Lagendijk, Phys. Rev. Lett. **83**, 2183 (1999).
[13] F. Scheffold, R. Lenke, R. Tweer, and G. Maret, Nature (London) **398**, 206 (1999).
[14] R. F. Potter, in *Handbook of Optical Constants of Solids*, edited by E. D. Palik (Princeton University Press, New York, 1952), p. 465.
[15] J. Gómez Rivas, R. Sprik, A. Lagendijk, L. D. Noordam, and C. W. Rella, Phys. Rev. E **62**, R4540 (2000).
[16] S. Glasstone and M. C. Edlund, *The Elements of Nuclear Reactor Theory* (Dover, New York, 1960).
[17] *Scattering and Localization of Classical Waves in Random Media*, edited by P. Sheng (World Scientific, New Jersey, 1990).
[18] J. H. Page, H. P. Schriemer, A. E. Bailey, and D. A. Weitz, Phys. Rev. E **52**, 3106 (1995).
[19] B. A. van Tiggelen, A. Lagendijk, M. P. van Albada, and A. Tip, Phys. Rev. B **45**, 12 233 (1992).
[20] E. Akkermans, P. E. Wolf, and R. Maynard, Phys. Rev. Lett. **56**, 1471 (1986).
[21] A. Lagendijk, R. Vreeker, and P. de Vries, Phys. Lett. A **136**, 81 (1989).
[22] J. X. Zhu, D. J. Pine, and D. A. Weitz, Phys. Rev. A **44**, 3948 (1991).
[23] A. Z. Genack and J. M. Drake, Europhys. Lett. **11**, 331 (1990).
[24] N. Garcia, A. Z. Genack, and A. A. Lisyansky, Phys. Rev. B **46**, 14 475 (1993).
[25] J. H. Li, A. A. Lisyansky, T. D. Cheung, D. Livdan, and A. Z. Genack, Europhys. Lett. **22**, 675 (1993).
[26] J. Gómez Rivas, R. Sprik, C. M. Soukoulis, K. Busch, and A. Lagendijk, Europhys. Lett. **48**, 22 (1999).
[27] E. Abrahams, P. W. Anderson, D. C. Licciardello, and T. V. Ramakrishnan, Phys. Rev. Lett. **42**, 673 (1979); P. Sheng, *Introduction to Wave Scattering, Localization, and Mesoscopic Phenomena* (Academic Press, New York, 1995).
[28] R. J. Hunter, *Foundations of Colloid Science* (Oxford University Press, Oxford, 1993), Vol. 2, p. 117.
[29] According to Mie scattering calculations, in the wavelength range of our experiments the scattering cross section σ_s of a Ge sphere of radius 0.19 μm in air is at least two orders of magnitude smaller than σ_s of a Ge sphere of radius 0.98 μm.
[30] D. Oepts, A. F. G. van der Meer, and P. W. Amersfoort, Infrared Phys. Technol. **36**, 297 (1995).
[31] C. F. Bohren and D. R. Huffman, *Absorption and Scattering of Light by Small Particles* (Wiley, New York, 1983), p. 217; S. Datta, C. T. Chan, K. M. Ho, and C. M. Soukoulis, Phys. Rev. B **48**, 14 936 (1993).
[32] J. Gómez Rivas, R. Sprik, A. Lagendijk, and C. W. Rella (unpublished).
[33] P. D. Kaplan, M. H. Kao, A. G. Yodh, and D. J. Pine, Appl. Opt. **32**, 3828 (1993).
[34] M. B. van der Mark, M. P. van Albada, and A. Lagendijk, Phys. Rev. B **37**, 3575 (1988); M. U. Vera, P.-A. Lemieux, and D. J. Durian, J. Opt. Soc. Am. A **14**, 2800 (1997).
[35] K. Busch and C. M. Soukoulis, Phys. Rev. Lett. **75**, 3442 (1995); A. Kirchner, K. Busch, and C. M. Soukoulis, Phys. Rev. B **57**, 277 (1998); C. M. Soukoulis, S. Datta, and E. N. Economou, *ibid.* **49**, 3800 (1994).
[36] J. Gómez Rivas, R. Sprik, and A. Lagendijk, Ann. Phys. (Leipzig) **8**, 77 (1999).
[37] R. H. J. Kop, P. de Vries, R. Sprik, and A. Lagendijk, Phys. Rev. Lett. **79**, 4369 (1997).
[38] Z. Q. Zhang, I. P. Jones, H. P. Schriemer, J. H. Page, D. A. Weitz, and P. Sheng, Phys. Rev. E **60**, 4843 (1999).